Particle Engulfment and Pushing by Solidifying Interfaces: Part II. Microgravity Experiments and Theoretical Analysis

D.M. STEFANESCU, F.R. JURETZKO, B.K. DHINDAW, A. CATALINA, S. SEN, and P.A. CURRERI

Results of the directional solidification (DS) experiments on particle engulfment and pushing by solidifying interfaces (PEP), conducted on the space shuttle Columbia during the Life and Microgravity Science (LMS) Mission, are reported. Two pure aluminum (99.999 pct) 9 mm cylindrical rods, loaded with about 2 vol pct 500-μm-diameter zirconia particles, were melted and resolidified in the microgravity (μg) environment of the shuttle. One sample was processed at a stepwise increased solidification velocity and the other at a stepwise decreased velocity. It was found that a pushing/engulfment transition (PET) occurred in the velocity range of 0.5 to 1 μm/s. This is smaller than the ground PET velocity of 1.9 to 2.4 μm/s. This demonstrates that natural convection increases the critical velocity. A previously proposed analytical model for PEP was further developed. A major effort to identify and produce data for the surface energy of various interfaces required for calculation was undertaken. The predicted critical velocity for PET was 0.775 μm/s.

I. INTRODUCTION

PARTICLE engulfment and pushing by solidifying interfaces (PEP) is one of the experiments presently scheduled to be conducted on the Space Station. An early flight opportunity provided by the Life and Microgravity Science (LMS) Mission on board the space shuttle Columbia (between June 22 and July 6, 1996) was used to run a limited number of experiments with metal-ceramic particle systems. The main objectives were as follows:(1) to evaluate the experimental method, including cartridge-sample design, thermal regime, velocity regime, and analysis procedures; (2) to obtain preliminary data on the critical velocity of particle engulfment; and (3) to demonstrate, by comparison with ground experiments, that liquid convection affects the critical velocity for engulfment.

This article includes the results obtained after 1 year of analysis of flight samples. An account of preflight ground results was presented in Part I of this article, so that an appropriate comparison can be made.

II. BACKGROUND

The physics of particle–solid/liquid (SL) interface interaction, when the interface approaches the particle with a solidification velocity V_{SL}, is summarized in Figure 1. Two distinct liquid flow patterns exist: flow into the interface generated by solidification and flow parallel to the interface at a velocity V_L induced by natural convection. Four main forces are identified: the interaction force between the particle and the SL interface (F_γ), typically a repulsive force; the drag force exercised by the solidification-induced liquid flow around the particle into the interface (F_D), which pushes the particle into the interface; the lift force produced by the liquid flow parallel to the interface (F_L), which pushes the particle away from the interface; and the gravity force (F_g). Considering the two velocities (V_{SL} and V_L), it can be rationalized that the behavior of the particle is governed by either the interface velocity or by the fluid flow velocity. Three regimes of particle-interface interaction can then be anticipated.

(1) no- or low-melt convection, $V > V_{cr}$ $\Rightarrow$ engulfment
(2) no- or low-melt convection, $V < V_{cr}$ $\Rightarrow$ pushing
(3) significant melt convection $\Rightarrow$ no particle-interface interaction

However, the V_{cr} changes when even low levels of convection are present in the liquid. Indeed, this behavior was demonstrated through experiments performed on transparent organic materials containing insoluble particles.[1]

Assuming steady state, that is, a very small particle acceleration from the time it starts ''feeling'' the interface to the time it is pushed by it, the pushing/engulfment transition (PET) can be described through a force balance,

$$F_D + F_g = F_L + F_\gamma \qquad [1a]$$

In a microgravity (μg) environment, the gravity and the lift forces can be ignored, so the problem simplifies to a balance between the drag and repulsive forces,

$$F_D = F_\gamma \qquad [1b]$$

Over the years, several steady-state models have been proposed to describe the PET. Most models[2–8] are based on various formulations of the forces in Eq. [1b]. The influences of melt convection and of the gravity force on the particle-interface interaction are ignored. The critical velocity calculated by these models is an inverse function of

D.M. STEFANESCU, University Research Professor and Director of Solidification Laboratory, and F.R. JURETZKO and A. CATALINA, Graduate Research Assistants, Metallurgical and Materials Engineering, are with The University of Alabama, Tuscaloosa, AL 35487. and B.K. DHINDAW, formerly Visiting Scholar, Solidification Laboratory, The University of Alabama, is Professor, IIT Kharagpur, India. S. SEN, Staff Scientist, USRA, and P.A. CURRERI, Metals and Alloys Group Leader and USMP Mission Scientist, are with the NASA Marshall Space Flight Center, Huntsville, AL 35806.

Manuscript submitted October 24, 1997.

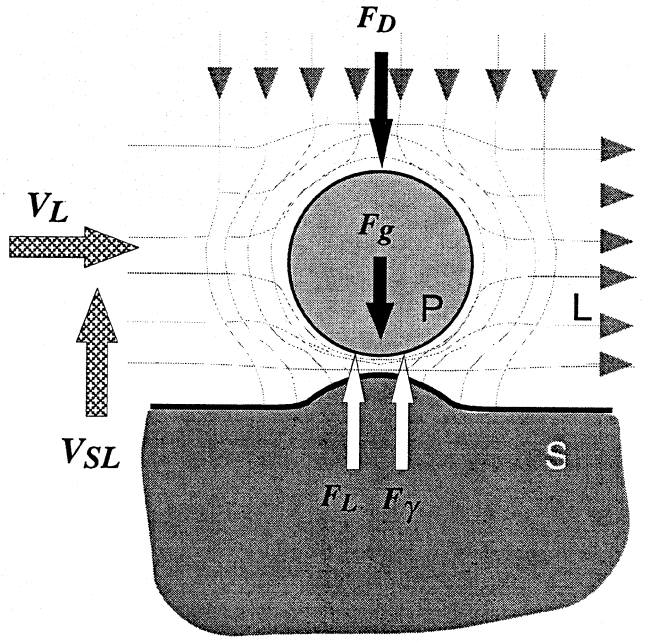

Fig. 1—Schematic representation of the forces acting on a particle in the vicinity of the solid-liquid interface.

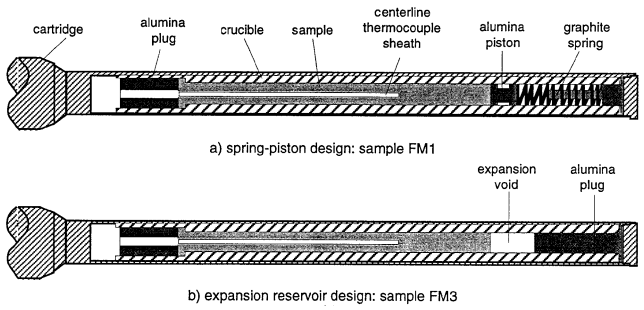

Fig. 2—(*a*) and (*b*) Design of cartridge-crucible-sample assembly.

particle radius at some power. To validate such models, μg experiments are required.

The complex issue of the effect of convective fluid flow on particle-interface interaction has not been addressed until recently. Han and Hunt[9] introduced in their analysis an additional force acting on a particle because of the difference in flow velocity in the region between the particle and the interface and in the region on the opposite side of the particle. This force acts normal to the interface, and its sign is determined by the direction of the fluid flow and the densities of the particle and the liquid. The critical velocity is calculated as a function of particle radius, solidification velocity, density difference, melt viscosity, and friction between the particle and the interface. However, because of the unavailability of data regarding fluid velocity during particle pushing experiments, this model is difficult to use.

In Part I of this article, the authors reported an experimental critical velocity for PET of 1.9 to 2.4 μm/s for the system Al/ZrO_2. The radius of the spherical zirconia particles was 250 μm. While this finding is important in terms of unequivocally establishing the value of critical velocity in a metal-ceramic system under ground conditions, it was believed that μg data must be generated for correct validation of existing steady-state models. Indeed, from Eq. [1a] it is seen that the lift force will behave like an additional repulsive force and, therefore, will alter the critical velocity. Thus, the hypothesis to be tested through μg experimentation is that the critical velocity in a μg environment should be different than the ground value.

III. EXPERIMENTAL WORK

During the LMS Mission, two samples were directionally solidified in the Advanced Gradient Heating Facility (AGHF). They will be referred to here as flight samples FM1 and FM3.

A. *Experimental Method*

The materials used for μg experimentation were the same as those for the ground experiments. They included 99.999 pct pure aluminum and spherical zirconia particles of 500-μm diameter.

The flight samples were prepared in the same way as the ground samples. However, three thermocouples were placed into a ceramic sheath along the centerline of each sample and incorporated by casting. Then the composite samples were introduced in alumina crucibles. An additional eight thermocouples were positioned in grooves on the outside of each crucible. Finally, the crucibles containing the samples were mounted into tantalum cartridges.

Unlike the vertical on-ground directional solidification (DS), during μg solidification the shrinkage cavity is not constrained to the top of the sample. Thus, obtaining a sound sample is not trivial. Consequently, to validate a cartridge-crucible-sample assembly for the Space Station experiment, two different cartridge designs were used (Figure 2). For sample FM1, the cartridge included an alumina piston and a graphite spring. The piston-spring system compensated for melting expansion and solidification shrinkage. A simpler design was used for sample FM3, in which an expansion reservoir was provided at the hot end of the crucible.

The samples were remelted and directionally solidified during flight in the AGHF. Since the number of samples to be processed was limited, and the quenching rate provided by the AGHF was not sufficient to conduct the DS experiments in a similar manner to the ground experiments, an alternative method for evaluation of the critical velocity was used. A three-step velocity profile was programmed into the furnace. For sample FM1, the furnace velocity was decreased from 20 to 5 and then to 0.5 μm/s. For sample FM3, the velocity was increased from 1 to 3 and then to 9 μm/s. Since it was possible to assess particle positions before remelting through X-ray transmission microscopy (XTM), the absence of particles in any of the directionally solidified zones was construed as particle pushing.

The flight data were recorded on a spreadsheet and included furnace position and velocity, thermocouple position, and temperature-time data. The SL interface velocity resulting from the different furnace translation velocities was calculated based on thermocouple data.

After μg processing, each cartridge was examined by X-ray computer tomography (XCT) to asses its integrity. Then, the crucibles were extracted from the cartridge. Each sample, still contained within the crucible, was studied, and

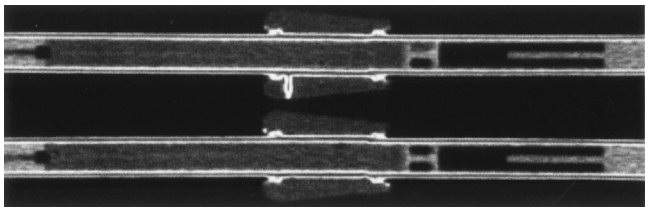

a) sample FM1

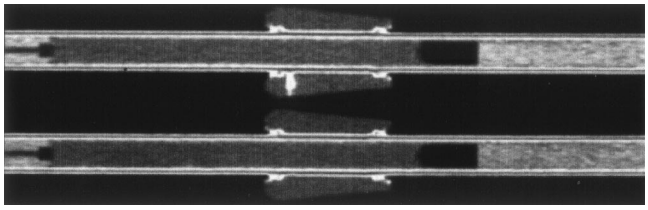

b) sample FM3

Fig. 3—(*a*) and (*b*) XCT images of the flight cartridge-crucible-sample assembly.

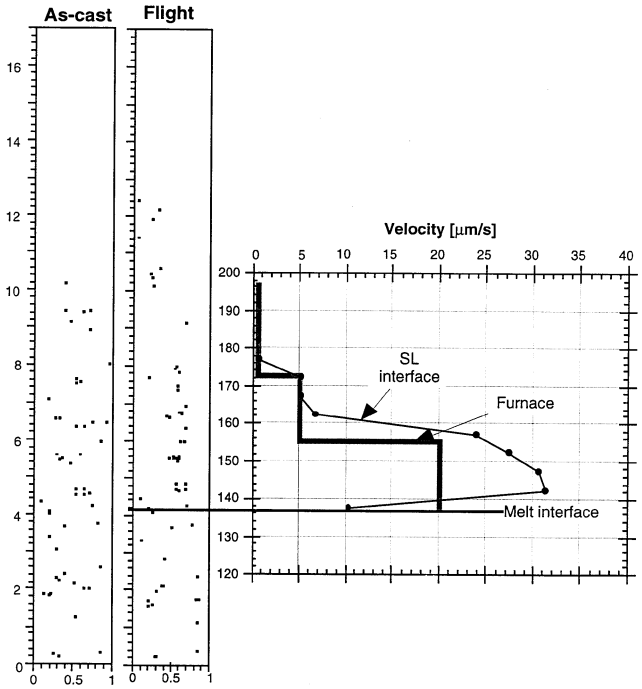

Fig. 4—Summary of XTM evaluation of particle positions correlated to furnace and solid/liquid interface velocity for sample FM1.

the images were recorded through XTM to assess the position of the particles with respect to the velocity zones.

B. *Experimental Results*

The results of the cartridge XCT evaluation are shown in Figure 3. The XCT shows the sample (gray), the crucible (white), the alumina plugs at the two ends of the crucible (light gray), and the liquid metal ring (LMR) around the crucible. The heat extraction by the LMR was used to improve the thermal gradient.

The spring-piston assembly used for sample FM1 functioned as expected. Some aluminum leakage is seen past the fore side of the piston. This leak is not significant. No aluminum is seen in the 90 deg position of the XCT (lower

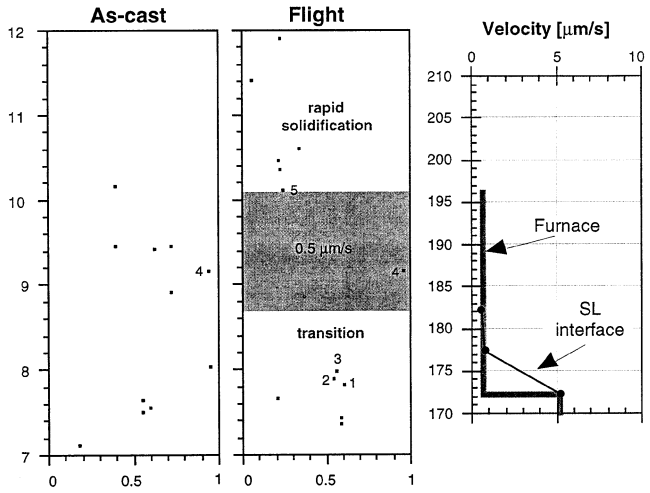

Fig. 5—Summary of XTM evaluation of particle positions in sample FM1 in the region of furnace translation rate of 0.5 μm/s.

picture on Figure 3(a)). No metal has leaked past the aft side of the piston, and the nominal operation of the spring-piston assembly was not affected. As a result, no void is seen between the piston and the sample. The sample itself was sound.

Sample FM3 also performed as expected. On Figure 3(b), it is seen that the shrinkage cavity remained between the metal and the alumina plug. The sample itself appears to have no significant shrinkage porosity or voids.

To evaluate the PET, particle positions in the sample established through XTM were correlated with the furnace velocity profile and with the SL interface position and velocity. A summary of XTM particle positions in the FM1 sample before and after flight is given in Figure 4. A number of particles are seen in the upper part of the flight sample. No corresponding particles are seen in the as-cast sample, simply because that part was not recorded. The two-dimensional representation of the spatial particle distribution is exact to ± 1 mm in the longitudinal axis of the sample. The width is enlarged by a factor of 2 to facilitate interpretation. To identify the particle positions with respect to velocity zones, a velocity-distance graph was associated with the XTM images. It is quite clear that, at velocities of 5 μm/s and above, all particles were engulfed. A more detailed analysis is necessary for the region solidified at 0.5 μm/s. To this effect, the region of interest was enlarged in Figure 5. It is seen that, in the transition zone where the SL interface velocity decreases from 5 to 0.5 μm/s, particles are still engulfed (particle nos. 1, 2, and 3). In the region of 0.5 μm/s, all particles have been pushed by the interface, with the exception of particle no. 4. However, upon rotating the sample during XTM examination, it was found that this particle is very close to the crucible wall, which means it should be removed from consideration. As soon as the velocity increases due to rapid furnace translation at the end of the experiment, particles are engulfed (no. 5). A detailed XTM image of the region of interest is presented in Figure 6.

The interface velocity could be accurately determined only as long as thermocouple information was available. Then, since in the 0.5 μm/s regime our calculations indicated that furnace velocity and interface velocity were lin-

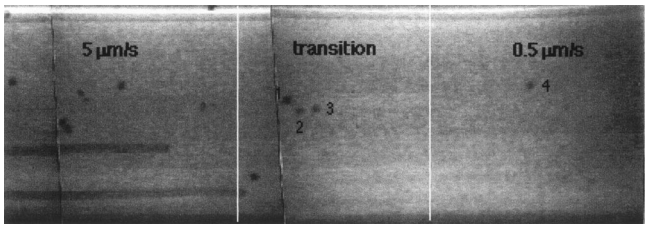

Fig. 6—XTM image of flight sample FM1. Particles are engulfed at 5 μm/s and in the transient region. No valid engulfed particles are present in the 0.5 μm/s region.

ear and had approximately the same slope, the velocity of the SL interface was assumed to be very close to that of the furnace for the remaining 0.5 μm/s zone.

From the XTM analysis of particle position in sample FM3 before and after flight (Figure 7) it is concluded that, since particles are found in all three velocity regions, engulfment occurred even at the lowest-velocity regime used in this sample, which was 1 μm/s.

C. *Discussion*

One of the basic criteria for acceptability of the PET experimental results is that the *particles* be *inert* with respect to the matrix. Thus, it must be documented that no reaction occurred at the particle/matrix interface. Selected results of scanning electron microscope evaluation of the particle/matrix interface in sample FM3 are presented in Figure 8. It is seen that, as long as moderate temperatures were reached during processing, a clean particle/matrix interface is obtained. The white borders on Figure 8(a) are only shadows, as demonstrated by EDX analysis. However, at temperatures higher than 950 °C, EDX analysis confirmed that zirconia particles reacted with the matrix, producing an oxidized Al_2O_3 interface (Figure 8 (b)). The temperature profile of the two flight samples showed that, in the region of controlled DS, the maximum temperature was 940 °C. Thus, it can be concluded that, in the region of interest, there was no particle-matrix reaction.

The flight results presented here seem to indicate that, for the Al-ZrO_2 system, the critical velocity for the PET is between 0.5 and 1 μm/s. The ground experiments presented in Part I of this article suggest a critical velocity between 1.9 and 2.4 μm/s. Thus, it is concluded that the absence of convection resulted in a decreased critical velocity. These results are in line with both fluid mechanics arguments and other experimental data.[10]

Indeed, assuming that the particle moves parallel to the SL interface because of natural convection (Figure 1), it can be expected to roll because of the velocity gradient imposed in the direction perpendicular to the interface. Simple calculations for ideal fluids show that in such a case a ''lift'' force will be generated.[11] This force will act perpendicular to the interface and will be directed away from it (note also the forces acting on the particle in Eq. [1a]). Work with organic transparent materials has also demonstrated that the critical velocity increases with the level of convection in the liquid and that, above a certain convection level, the particle does not interact with the interface at all.[1]

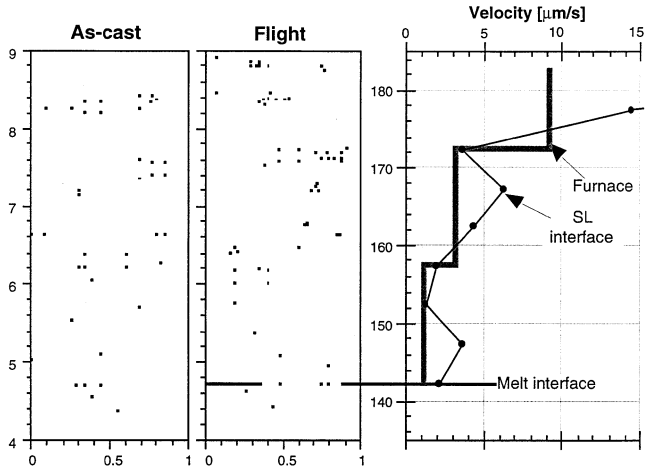

Fig. 7—Summary of XTM evaluation of particle positions in sample FM3 in the region of furnace translation rates of 1 and 3 μm/s.

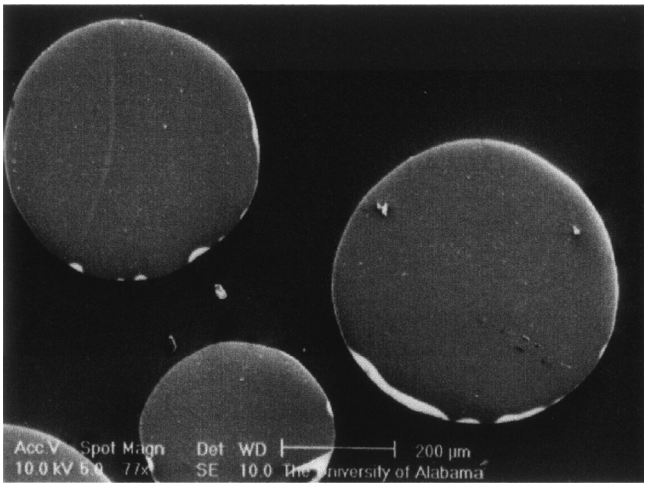

a) good interface in the DS region at 710 °C

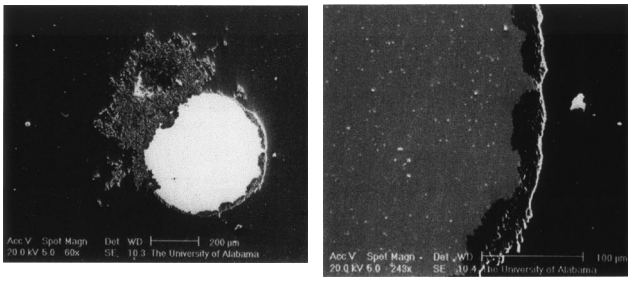

b) oxidized interface in DS region at 950 °C

Fig. 8—(*a*) and (*b*) SEM evaluation of particle (zirconia)-matrix (A1) interface in sample FM3.

IV. THEORETICAL ANALYSIS

In this section, it will be attempted to demonstrate that, while analytical models have clear limitations, they can predict reasonably well the experimental data presented in this article. The main model to be tested is that previously developed by some of the authors[5,6] and further refined in this article. Other models will also be included in this discussion for comparison.

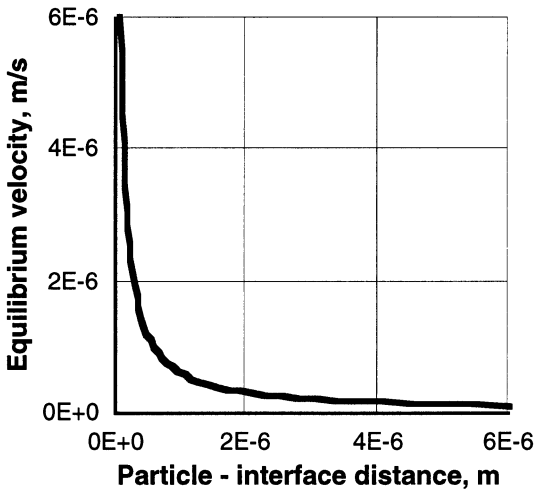

Fig. 9—Equilibrium velocity-distance from interface correlation for a zirconia particle in an aluminum matrix.

A. *Model Development*

In the original model by Shangguan *et al.* (SAS),[6] an equilibrium velocity was defined based on Eq. [1b]. The two forces in this equation were derived to be

$$F_D = 6\pi\eta V_{SL}\frac{R^2}{d}K^{*2} \qquad [2]$$

$$F_\sigma = 2\pi R\Delta\sigma_0\left(\frac{a_0}{a_0 + d}\right)^n K^* \qquad [3]$$

where η is the liquid viscosity, R is the particle radius, $K^* = K_P/K_L$ is the ratio between the thermal conductivity of the particle (K_P) and of the liquid (K_L), a_0 is the atomic diameter, d is the equilibrium distance, and n is an exponent that can have values between 2 and 7. Also, $\Delta\sigma_0$ was defined as[12]

$$\Delta\sigma_0 = \sigma_{PS} - \sigma_{PL} - \sigma_{LS} \qquad [4]$$

where σ stands for the surface tension of the solid (S), liquid (L), and particle (P), respectively.

Assuming steady state, when the two forces described by the previous equations are equal, the particle will not change its position with respect to the interface. This means that the particle is pushed at a velocity equal to the solidification velocity. This is the equilibrium velocity, and can be calculated as

$$V_{eq} = \frac{\Delta\sigma_0 d}{3\eta K^* R}\left(\frac{a_0}{a_0 + d}\right)^n \qquad [5]$$

However, engulfment is not a steady-state event, since the particle is accelerated with respect to the interface at the beginning of the interaction and this acceleration changes continuously when the particle is engulfed. A steady state may occur only during pushing. Consequently, this equation cannot directly give the critical velocity. In the SAS model, the critical velocity was obtained by maximizing this equation with respect to d, which implies the assumption that the minimum distance is $d = a_0$. At the time this work was performed, calculation of $\Delta\sigma_0$ was uncertain, and, thus, $\Delta\sigma_0$ was used as a fitting parameter for validation.

In a recent article, Sen *et al.*[1] argued that it is hard to accept a critical distance on the order of the atomic distance. Based on a discussion by Cottrell,[13] who suggested that the typical properties of the metal cannot be obtained in cluster smaller than a specific size, they proposed a critical distance on the order $d_{cr} = 50\ a_0$. Further assuming that $n = 2$, the critical velocity was written as

$$V_{cr} = \frac{0.0064\ \Delta\sigma_0 a_0}{\eta K^*\ R} \qquad [6]$$

A methodology for calculation of $\Delta\sigma_0$ was also outlined.

A further enhancement of the SAS model will now be introduced. First, the surface tension difference is replaced by the surface energy difference, given by

$$\Delta\gamma_0 = \gamma_{PS} - \gamma_{PL} \qquad [7]$$

The rationale for this change is discussed in the Appendix. Also in the Appendix, it is demonstrated that the value of the exponent in the interaction force equation is $n = 2$. With these changes, the equilibrium velocity becomes

$$V_{eq} = \frac{\Delta\gamma_0 a_0^2}{3\eta K^*\ R}\frac{1}{d} \qquad [8]$$

This equation describes a hyperbolic correlation between the interface velocity and particle-interface distance. For the Al-ZrO_2 system (250-μm-radius particles), this dependency is shown in Figure 9. It is seen that, as the particle approaches the interface (d decreases), at the beginning V_{eq} increases very little. In this region, the particle acceleration resulting from the force difference F_D-F_γ is minimal, and the assumption of steady state is reasonable. However, when the apex of the hyperbola is reached, for a small change in d, a dramatic increase in V_{eq} results. When the particle approaches the interface at velocities larger than that of the apex, calculation shows that, before equilibrium could be reached, $F_D >> F_\gamma$. The acceleration is very large, and steady state cannot be established. Consequently, the V_{eq}-d curve is invalid at velocities higher than that of the apex. Thus, the equilibrium velocity corresponding to the apex is the smallest possible pushing velocity and is, therefore, the critical velocity.

Having assumed that the critical velocity is that at the apex of the hyperbola describing the V_{eq}-d correlation, the value of the critical velocity can be calculated as follows. From the first derivative of Eq. [8],

$$d = \left[-\frac{\Delta\gamma_0 a_0^2}{3\eta K^*\ R}\left(\frac{\mathrm{d}V}{\mathrm{d}d}\right)^{-1}\right]^{1/2}$$

Then, the critical distance and the critical velocity are, respectively,

$$d_{cr} = \left[-\frac{\Delta\gamma_0 a_0^2}{3\eta K^*\ R}\left(\frac{\mathrm{d}V}{\mathrm{d}d}\right)_{cr}^{-1}\right]^{1/2} \text{ and}$$

$$V_{cr} = \left[-\frac{\Delta\gamma_0 a_0^2}{3\eta K^*\ R}\left(\frac{\mathrm{d}V}{\mathrm{d}d}\right)_{cr}\right]^{1/2}$$

Since at the apex of the hyperbola $(\mathrm{d}V/\mathrm{d}d)_{cr} = -1$ (note that the units are s^{-1}), the critical velocity is

$$V_{cr} = \left(\frac{\Delta\gamma_0 a_0^2}{3\eta K^*\ R}\right)^{1/2} \qquad [9]$$

Table I. Interfacial Energies in the Al - ZrO_2 and Zn - ZrO_2 Systems

Energy, J/m²	Al - ZrO_2	Source	Zn - ZrO_2	Source
γ_{PV}	0.697	18, 19	0.697	18, 19
γ_{LV}	0.870	20	0.770	21
γ_{SV}	0.896	21	0.895	22
γ_{PL}	1.450	Eq. [10], $\theta = 150$, Ref. 23	1.022	Eq. [10], $\theta = 115$ deg
γ_{PS}	1.593	Eq. [13], $a = 0$	1.592	Eq. [13], $a = 0$
$\Delta\gamma_0$	0.143	Eq. [17]	0.570	Eq. [17]

B. *Calculation of Surface Energies*

To unambiguously validate PET models against the experimental data presented in Parts I and II of this article, it is necessary to accurately evaluate the various thermophysical parameters that determine the values of the interacting forces. There is a clear lack of data and/or methodology for such an evaluation (note, for example, Reference 14). The drag force can be accurately calculated, as parameters such as melt viscosity and particle radius are well quantified. Even contribution from localized distortions of the SL interface due to differences in thermal conductivities between melt and particles have been theoretically analyzed in several models.[4,6] The repulsive force in most models originates from the difference in surface energies between the particle and the matrix material. Accurate calculations are lacking because of the unavailability of relevant data such as interfacial energies between the solid/vapor, particle/vapor, and/or solid/particle. This article addresses these issues by developing the data and a methodology for the calculation of interface energies.

In the proposed model, the calculation of the critical velocity is based upon the surface energy difference ($\Delta\gamma_0$). Thus, the values of γ_{PS} and γ_{PL} are needed.

The value of γ_{PL} can be calculated from Young's equation,

$$\gamma_{PL} = \gamma_{PV} - \gamma_{LV} \cos\theta \qquad [10]$$

Both γ_{PV} and γ_{LV} are typically available in the literature, being directly measured for many systems. The contact angle θ can be measured using sessile drop experiments.

The evaluation of γ_{PS} is more complicated. A number of researchers have used the following generic equation of state proposed by Neumann and co-workers[15,16] for a two-component, three-phase system:

$$\gamma_{12} = \frac{(\gamma_{13}^{1/2} - \gamma_{23}^{1/2})^2}{1 - K_0 (\gamma_{13}^{1/2} - \gamma_{23}^{1/2})} \qquad [11]$$

where 1, 2, and 3 are three different phases in contact with each other, and K_0 is a material constant. For this problem, the phases of interest are the particle, liquid, solid, and vapor (V) phases; they can be used in any order. For organic systems, Neumann *et al.* give a value of $K_0 = 0.015$, based on experimental data. For metal-ceramic systems K_0 values can be calculated with the previous equation for the S, L, and V phases. Then, the same equation is used to calculate γ_{PS}. However, the uncertainty in the values of interface energies for metals and ceramics results in slight variations in the calculated value of K_0. It can be easily demonstrated that changes in the K_0 value on the order of 0.001 result in significant changes of γ_{PS}. Accordingly, this method cannot be used unless a significant amount of data exist to evaluate K_0, as was done for the case of organic materials. In the absence of such data, this method must be considered as unreliable.

Another approach to the calculation of γ_{PS} is by using the work of adhesion. The underlying assumption behind this approach is that when two solids that are in contact are separated because of the creation of two new solid-vapor interfaces, the interface energy in the system is increased by the work of adhesion,

$$\gamma_{PS} = \gamma_{PV} + \gamma_{SV} - W_{ad-PS} \qquad [12]$$

The work of adhesion could be calculated from the Girifalco–Good relationship.[17] However, this relationship was derived on the basis of polar forces between molecular liquids, and its applicability for this case is questionable. Furthermore, the problem is complicated by the fact that solidification of the matrix around the particle may produce some strain because of the difference in the expansion coefficients of the two solids. This analysis is valid, assuming perfect contact between the matrix and the particle. Such contact is improbable for nonwetting systems. To account for the the strain and the imperfect contact, this equation must be modified as follows:

$$\gamma_{PS} = \gamma_{PV} + \gamma_{SV} - a(W_{ad} + W_{str}) \qquad [13]$$

where W_{str} is the energy introduced by the thermal mismatch; $a = 0$ for no contact, and $a = 1$ for perfect contact. It is reasonable to assume that, for rough particles that are not wetted by the liquid, as is the case for most ceramic particles in contact with liquid metals, a will be closer to 0 than to 1.

In many instances, the value of γ_{PV} and γ_{SV} can be found in the literature. The value of γ_{SV} may also be calculated from the heat of sublimation, with the equation[21]

$$\gamma_{SV} = 0.16\ \Delta H_{vap}$$

The relevant interface energies, as well as the sources used for the Al-ZrO_2 and Zn-ZrO_2 systems, are summarized in Table I.

The calculation of $\Delta\gamma_0$ in Table I was done assuming poor particle-solid contact. The case must then be made for poor contact between the engulfed zirconia particle and the surrounding aluminum matrix. Indeed, as shown in Figure 10, upon fracture, the zirconia particle is pulled out of the matrix, leaving very limited particle-solid contact. Since the aluminum-zirconia contact angle measurements performed in our laboratory also showed poor contact (the solidified aluminum sessile drop did not adhere at all to the zirconia substrate), it is reasonable to conclude that a should be nearer to 0 than to 1. Thus, in further calculations, the values of $\Delta\gamma_0$ resulting from $a = 0$ were adopted for both the aluminum and zinc matrices.

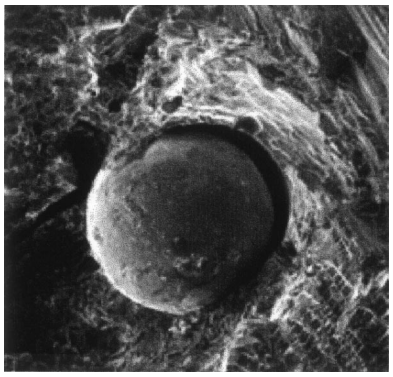

Fig. 10—Scanning electron micrograph of a fracture surface from a directionally solidified aluminum-zirconia sample.

C. *Comparison of Experimental Results and Model Predictions*

1. *Models tested*

Analytical PET models cannot describe natural convection. Thus, the underlying assumption is that of no convection. The *no-convection* models differ mostly in the assumptions made regarding the repulsive (interface interaction) force. Several models have been proposed for the interface interaction force.

The Uhlmann, Chalmers, and Jackson (UCJ) model[12] is based on the assumption that the interfacial repulsive force is due to the variation of the surface free energy, described by Eq. [4], with the distance d (Eq. [3]). The value of the exponent n is uncertain, and it was assumed to be between 4 and 5. The controlling transport mechanism in the particle-interface gap was assumed to be mass diffusion. The critical velocity was derived as

$$V = \frac{n+1}{2}\left(\frac{\Delta H_f\, a_0 \Omega D}{k_B T R^2}\right) \qquad [14]$$

where ΔH_f is the latent heat of fusion, Ω is the atomic volume, D is the liquid diffusivity, k_B is the Boltzman's constant, and T is the temperature.

In the formulation by Chernov, Temkin, and Mel'nikova (CTM),[2,3] it is assumed that, as the interface approaches the particle, the difference in chemical potential between the liquid and the particle produces a repulsive force (''disjoining pressure''). The critical velocity for metallic systems has been derived to be

$$V_{cr} = \frac{0.14 B^{2/3}\, \sigma_{SL}^{1/3}}{\mu R^{4/3}} \quad \text{for small particles } (R < 500\ \mu\text{m}) \qquad [15]$$

where B is a constant defining the disjoining pressure, ΔS_f is the entropy of fusion, and G is the temperature gradient in the liquid. For dielectrics, a different constant B is used, but the equation for critical velocity has never been derived. The weakness of this model is in the difficulty of assigning a value to the constant B. Indeed, according to CTM, ''the strict calculation of B is impossible.'' Based on a number of assumptions difficult to verify, they produce an approximate and universal value of $B = 10^{-21}$ J, independent of the system.

Table II. Parameters Used for Theoretical Calculations of Critical Velocity in the Aluminum-Zirconia and Zinc-Zirconia Systems

Parameter	Al - ZrO_2	Reference	Zn - ZrO_2	Reference
η ($N\cdot m^{-1}\cdot s^{-1}$)	$1.18\cdot10^{-3}$	24	$3.5\cdot10^{-3}$	25
D ($m^2\cdot s^{-1}$)	$4.87\cdot10^{-9}$	25	$2.03\cdot10^{-9}$	25
γ_{SL} ($J\cdot m^{-2}$)	0.121	21	0.179	estimated 21
$\Delta\gamma_0$ ($J\cdot m^{-2}$)	0.143	this work	0.570	this work
B (J)	10^{-21}	3	10^{-21}	3
Ω ($m^3\cdot at^{-1}$)	$1.88\cdot10^{-29}$	25	$1.59\cdot10^{-29}$	25
a_0 (m)	$2.86\cdot10^{-10}$	24	$2.78\cdot10^{-10}$	24
ΔH_f ($J\cdot m^{-3}$)	$9.45\cdot10^{8}$	26	$6.64\cdot10^{8}$	26
K_P ($W\cdot m^{-1}\cdot K^{-1}$)	1.97*	27	1.84*	27
K_L ($W\cdot m^{-1}\cdot K^{-1}$)	90.7	28	49.5	28

*At melting point of matrix.

Table III. Summary of Experimental and Calculated Critical Velocities (μm/s)

Particle Radius, μm	Al - ZrO_2 Experimental Ground	Al - ZrO_2 Experimental μg	Al - ZrO_2 Proposed Model	Al - ZrO_2 UCJ	Al - ZrO_2 CTM
100	—	—	1.225	$2.88\cdot10^{-4}$	0.127
250	1.9 to 2.4	0.5 to 1.0	0.775	$4.61\cdot10^{-5}$	0.038
400	—	—	0.613	$1.80\cdot10^{-5}$	0.020
	Zn - ZrO_2				
100	—	—	1.062	$9.35\cdot10^{-5}$	0.049
250	1.9 to 2.9	—	0.672	$1.50\cdot10^{-5}$	0.014
400	—	—	0.531	$5.84\cdot10^{-5}$	0.008

2. *Validation*

The experimental results will be compared with predictions by the model previously proposed in this article (proposed model), as well as by the UCJ and CTM models. The values for the quantities required for model validation are listed in Table II.

The experimental and calculated critical velocities for PET are given in Table III. The value of 0.775 μm/s calculated with the proposed model for the Al-ZrO_2 system for a particle radius of 250 μm fits right between the experimental μg values. It is smaller than the ground experiment value. This is expected. Indeed, when analyzing Eqs. [1a], [2], and [3], it is seen that a lift force (F_L) produced by natural convection should increase the critical velocity. Since the model as well as the μg experiment exclude the occurrence of natural convection at the SL interface, the critical velocity should be lower than that measured on ground. A reasonable critical velocity is also predicted for the Zn-ZrO_2 system. It is slightly lower than the ground value, again, as expected.

The CTM model predicts a critical velocity smaller by one order of magnitude than the experimental data. The UCJ model is several orders of magnitude smaller. This is probably because one of the basic assumptions of the UCJ model is that transport in the particle-interface gap is by diffusion only. Since the particle-SL interface gap is roughly 0.5 μm, mass transport is by fluid flow and diffusion. Since the former is much faster, the PET model must be based on transport by fluid flow rather then by diffusion.

V. CONCLUSIONS

In-flight DS experiments were conducted to evaluate the PET for pure aluminum (99.999 pct) doped with spherical zirconia particles. Two 9-mm cylindrical rods, loaded with about 2 vol pct 500-μm-diameter zirconia particles, were melted and resolidified in the (μg) environment of the shuttle. The position of the particles before and after processing was evaluated through XTM. It was found that a PET occurred in the velocity range of 0.5 to 1 μm/s. This is smaller than the ground PET velocity of 1.9 to 2.4 μm/s. This demonstrates that, as predictable from the theory, natural convection increases the critical velocity.

The SAS model was further developed. It was unambiguously demonstrated that the value of the exponent n, previously assumed to be 2, is indeed 2. The critical velocity and the critical distance were calculated based on the minimum equilibrium velocity at which the steady-state assumption is still valid. A methodology for evaluation of the surface energy of various interfaces required for calculation was described. The predicted critical velocity for PET was 0.775 μm/s. It agrees very well with that obtained during μg experimentation.

ACKNOWLEDGMENTS

This work has been supported by NASAs Microgravity and Applications division through Grant No. NAS8-39715. Dr. W. Kaulker's interest in the work and help with the XTM sample evaluation are gratefully acknowledged. R. Spivey and S. Breeding were extremely helpful during the flight integration of the experiment. The cartridges were manufactured by SOTEREM (Toulouse, France) and the flight integration was supported by CNES (Toulouse, France). The following individuals deserve particular recognition for their contributions: Helen Ben-Aïm, A. Desroches, and J.P. Pissard. The AGHF team, led by J. Ströde, has also been very helpful during these experiments.

LIST OF SYMBOLS

a	coefficient (0 for no contact and 1 for perfect contact)
a_0	atomic diameter
A	Hammaker constant
B	constant defining the disjoining pressure (CTM model)
d	equilibrium distance
d_{cr}	critical distance
D	liquid diffusivity
E_{vdW}	van der Waals energy
F_g	gravity force
F_D	drag force
F_L	lift force
F_{vdW}	van der Waals force
$F_{\gamma,\sigma}$	interaction force between the particle and the SL interface
G	temperature gradient in the liquid (CTM model)
ΔH_f	latent heat of fusion
ΔH_{vap}	heat of sublimation
k_B	Boltzman's constant
K_0	material constant
K^*	ratio between the thermal conductivity of the particle (K_P) and of the liquid (K_L)
n	exponent between 2 and 7 (UCJ and SAS models)
R	particle radius
ΔS_f	entropy of fusion
T	temperature
V	velocity
V_{cr}	critical velocity
V_L	fluid velocity at the SL interface parallel to the interface
V_{SL}	solidification velocity
W_{ad}	work of adhesion
γ	surface energy
η	liquid viscosity
θ	contact angle
σ	surface tension
$\Delta\sigma_0$	surface tension difference
$\Delta\gamma_0$	surface energy difference
Ω	atomic volume
Ψ ($\propto$)	function with value of 0.34

Subscripts

L	liquid (matrix)
P	particle
S	solid (matrix)

APPENDIX

This discussion is undertaken in an attempt to clarify the value of the exponent n in the models, using the decay of interface energy with distance to explain the origin of the repulsive force (*e.g.*, the UCJ and SAS models).

The expression for $\Delta\sigma_0$ and the local force during engulfment, as proposed by UCJ and adopted by SAS, can be derived[29] by writing an energy balance for the case in Figure A1,

$$G_\sigma = 2\pi R x \sigma_{PS} + 2\pi R\,(2R - x)\,\sigma_{PL} + \pi(R - x)^2\,\sigma_{SL}$$

The force at $x = 0$ resulting from this energy is

$$F_\sigma = \left.\frac{dG_\sigma}{dx}\right|_{x=0} = 2\pi x \sigma_{SL} + 2\pi R\,(\sigma_{PS} - \sigma_{PL} - \sigma_{SL}) = 2\pi R \Delta\sigma_0 \quad [A1]$$

It can then be assumed to decay in front of the interface following an exponential function (Eq. [3]). This derivation is true when surface tension, rather than surface energy, is used.

The relevance of the term σ_{SL} is questionable, since both the initial and final states include this term. Thus, the dif-

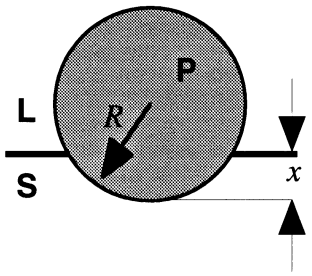

Fig. A1—Particle being engulfed.

ference in free energy between the particle being in the liquid and the particle being in the solid is simply

$$\Delta G = 4\pi R^2 \Delta\gamma_0 \text{ where } \Delta\gamma_0 = \gamma_{PS} - \gamma_{PL} \quad [A2]$$

We will use this equation to describe the variation of interface energy with distance ahead of the interface. The value of the exponent n is still to be determined.

The average interaction force resulting from the difference in interface energy can be calculated as

$$\overline{F_\gamma} = \frac{\Delta G}{2R + a_0} = 4\pi \Delta\gamma_0 \frac{R^2}{2R + a_0} \approx 2\pi R \Delta\gamma_0 \quad [A3]$$

The nonretarded van der Waals potential between two spheres of equal size, assuming small interparticle separation ($d << R$), is[30]

$$E_{\text{vdW}} = -\frac{A}{12} R d^{-1}$$

where A is the Hammaker constant. The interaction force between two particles is

$$F_{\text{vdW}} = \frac{dE_{\text{vdW}}}{dd} = \frac{A}{12}\frac{R}{d^2}$$

Also, it was demonstrated that the van der Waals interaction force between a sphere and a plane surface is[31]

$$F_{\text{vdW}} = \frac{2}{3} A \frac{R^3}{(a_0 + d)^2 (a_0 + d + 2R)^2} \quad [A4]$$

If the particle and the plane are of the same material, the van der Waals interaction is always attractive. For different materials, it can be either attractive or repulsive.[31] To find the Hammaker constant, we will assume that the origin of the repulsive force is in the difference in surface energy (Eq. [17]). This is a reasonable assumption for metal-ceramic systems when the liquid metal does not wet the ceramic and there is no chemical interaction. If chemical interaction occurs, this derivation does not hold.

Equating Eqs. [18] and [19] for the minimum separation distance between the particle and the interface a_0 ($d = 0$), and since $a_0 << R$, we obtain

$$A = 12\pi a_0^2 \Delta\gamma \quad [A5]$$

Let us calculate the value of the Hammaker constant. For the biphenyl/nylon, biphenyl/acetol, naphthalene/nylon, and naphthalene/acetol systems, the difference in surface energy, according to Reference 32, is $\Delta\gamma = 2.1$ to $2.7 \cdot 10^{-3}$ J/m^2. Taking the atomic distance $a_0 = 5 \cdot 10^{-10}$ m, the Hammaker constant is $A = 1.98$ to $2.5 \cdot 10^{-20}$ J. This is a very reasonable value, since the Hammaker constants for single materials usually vary between 10^{-20} and 10^{-19} J[30].

The interface repulsive force can now be obtained by combining Eqs. [19] and [20].

$$F_\gamma = 2\pi R \Delta\gamma_0 \left(\frac{a_0}{a_0 + d}\right)^2 = 2\pi R \Delta\gamma \quad [A6]$$

where

$$\Delta\gamma = \Delta\gamma_0 \left(\frac{a_0}{a_0 + d}\right)^2$$

Thus, it is apparent that, when van der Waals interaction is assumed between a spherical particle and a planar interface and the origin of the repulsive force is considered to be the difference in interface energy, the exponent in Eq. [3] is $n = 2$.

Since typically $a_0 << d$, the interface force becomes

$$F_\gamma = 2\pi \Delta\gamma_0 \left(\frac{a_0}{d}\right)^2 R \quad [A7]$$

To summarize, the main differences between the proposed model for the particle-interface interaction force and the UCJ and SAS models are that, for the new model surface energy, $\Delta\gamma_0 = \gamma_{PS} - \gamma_{PL}$ rather than the surface tension is used (as resulting from the derivation of the repulsive force), and the value of the exponent in the power law defining the variation of interface energy with distance is $n = 2$.

REFERENCES

1. S. Sen, B.K. Dhindaw, D.M. Stefanescu, A. Catalina, and P.A. Curreri: *J. Cryst. Growth*, 1997, vol. 173, pp. 574-84.
2. A.A. Chernov, D.E. Temkin, and A.M. Mel'nikova: *Sov. Phys. Crystallogr.*, 1977, vol. 22 (6), pp. 656-58.
3. A.A. Chernov, D.E. Temkin, and A.M. Mel'nikova: *Sov. Phys. Crystallogr.*, 1976, vol. 21 (4), pp. 369-74.
4. G.F. Bolling and J.A. Cissé: *J. Cryst. Growth*, 1971, vol. 10, pp. 56-66.
5. D.M. Stefanescu, B.K. Dhindaw, S.A. Kacar, and A. Moitra: *Metall. Trans. A*, 1988, vol. 19A, pp. 2847-55.
6. D.K. Shangguan, S. Ahuja, and D.M. Stefanescu: *Metall. Trans. A*, 1992, vol. 23A, pp. 669-80.
7. C. Körber, G. Rau, M.D. Causman, and E.G. Cravalho: *J. Cryst. Growth*, 1985, vol. 27, pp. 649-62.
8. J. Pötschke and V. Rogge: *J. Cryst. Growth*, 1989, vol. 94, pp. 726-38.
9. Q. Han and J.D. Hunt: *Iron Steel Inst. Jpn. Int.*, 1995, vol. 35 (6), pp. 693-94.
10. R.B. Fedich and W.R. Wilcox: *Sep. Sci. Technol.*, 1980, vol. 15 (1), pp. 31-38.
11. R.H. Nunn: *Intermediate Fluid Mechanics*, Hemisphere Publishing Co., New York, NY, 1989, pp. 51-55.
12. D.R. Uhlmann, B. Chalmers, and K.A. Jackson: *J. Appl. Phys.*, 1964, vol. 35, pp. 2986-93.
13. A. Cottrell: *Introduction to the Modern Theory of Metals*, The Institute of Metals, London, 1988.
14. P.K. Rohatgi, S. Ray, R. Asthana, and C.S. Narendranath: *Mater. Sci. Eng.*, 1993, vol. A162, pp. 163-74.
15. A.W. Neumann, R.J. Good, C.J. Hope, and M. Sejpal: *J. Colloid Interface Sci.*, 1974, vol. 69 (2), pp. 291-302.
16. S.N. Omenyi, A.W. Neumann, and C.J. Van Oss: *J. Appl. Phys.*, 1981, vol. 52 (2) pp. 789-95.
17. A.W. Adamson: *Physical Chemistry of Surfaces*, John Wiley & Sons, Inc., New York, NY, 1982.
18. D.T. Livey and P. Murray: *J. Am. Ceramic Soc.*, 1956, vol. 39 (11), pp. 363-72.
19. W.D. Kingery: *J. Am. Ceramic Soc.*, 1954, vol. 37 (2), pp. 42-45.
20. S.H. Overbury, P.A. Bertrand, and G.A. Somorjai: *Chem. Rev.*, 1975, vol. 75 (5), pp. 547-57.
21. L.R. Murr: *Interfacial Phenomena in Metals and Alloys*, Addison-Wesley, Reading, MA, 1975.
22. A.A. Chernov: private communication, University Space Research Association, Huntsville, AL, 1997.
23. J.G. Li: *Ceram. Int.*, 1994, vol. 20, pp. 391-412.
24. *CRC Handbook of Chemistry and Physics*, 67th ed., R.C. Weast, ed., CRC Press Inc., Boca Raton, FL, 1986.
25. T. Iida and R.I.L. Guthrie: *The Physical Properties of Liquid Metals*, Clarendon Press, Oxford, United Kingdom, 1988.
26. *ASM Handbook*, ASM INTERNATIONAL, Materials Park, OH, 1990, vol. 2, pp. 1099-1201.
27. *Thermophysical Properties of High Temperature Solid Materials*,

Y.S. Touloukian, ed., The Macmillan Company, New York, NY, vol. 4.
28. Y.S. Touloukian, R.W. Powell, C.Y. Ho, and P.G. Klemens: *Thermophysical Properties of Matter*, IFI/Plenum, New York, NY, 1970, vol. 1.
29. G. Kaptay: *Mater. Sci. Forum*, 1994, vol. 20, pp. 467-74.
30. D.J. Shaw: *Introduction to Colloid and Surface Chemistry*, Butterworth and Co., London, 1980.
31. D. Langebin: in *Intermolecular Forces*, B. Pullman, ed., Reidel, Dordrecht, Netherlands, 1981, p. 547.
32. S.N. Omenyi and A.W. Neumann: *J. Appl. Phy.*, 1976, vol. 47, p. 3956.